Ultra-wideband antenna system for in-band full-duplex applications

Hadi Hijazi, Marc Le Roy, Raafat Lababidi, Denis Le Jeune, André Pérennec

IET Microwaves, Antennas & Propagation

The Institution of Engineering and Technology WILEY

ORIGINAL RESEARCH PAPER

Ultra-wideband antenna system for in-band full-duplex applications

Hadi Hijazi[1,2] | Marc Le Roy[2] | Raafat Lababidi[1] | Denis Le Jeune[1] | Andre Pérennec[2]

[1]ENSTA Bretagne, Lab-STICC, CNRS, Brest, France

[2]Univ Brest, Lab-STICC, CNRS, Brest, France

Correspondence

Hadi Hijazi, ENSTA Bretagne, Lab-STICC, CNRS, UMR 6285, F-29200 Brest, France.
Email: hadi.hijazi@ensta-bretagne.org

Abstract

In this study, we present an ultra-wideband full-duplex system constituted of a wideband 4-element Vivaldi array and wideband microstrip-to-slotline baluns. The proposed system is characterised by its simplicity, high directivity, and high self-interference cancellation levels over a wide frequency bandwidth. The system is fabricated using basic printed-circuit board (PCB) technology and can provide at least 50 dB of self-interference cancellation over the bandwidth of operation, 4–40 GHz, with an average gain of 7.8 dBi. The system has a size of 8 cm × 8 cm × 9.4 cm and can be used as a high data rate link between two distant wireless nodes. To assess the merits of the proposed system and compare it to other published works, a new figure of merit (FoM$_{WFD}$) dedicated to wide-band full-duplex antenna topologies is introduced in this study.

KEYWORDS

baluns, microstrip transitions, ultra wideband antennas, Vivaldi antennas

1 | INTRODUCTION

Estimates of future mobile traffic indicate that the global number of mobile subscriptions could be 13.8 billion in 2025 and 17.1 billion in 2030 [1]. The increase in the number of mobile users creates a spectrum congestion problem and elevates the pressure on the available mobile infrastructure to keep up with the increased demand for mobile services. These problems create the need for new approaches to find more spectrum resources by improving traditional spectrum sharing techniques and/or harnessing new ones. Recently, in-band full-duplex (IBFD) technology emerged as a promising solution for the spectrum congestion problem [2]. As opposed to the traditional out-of-band full-duplex (OBFD), which utilises orthogonal resources (frequency or time) to establish a full-duplex communication, in-band full-duplex allows the simultaneous transmission and reception between two communicating nodes at the same frequency and the same time slot. This can only be achieved by reducing the self-interference signals that are coupled from the transmitter of one node to its own receiver below the noise floor level, allowing the receiver to receive the useful signal transmitted by the other node. Nominally, 110 dB of self-interference cancellation is required to be able to establish an in-band full-duplex communication [3].

Figure 1 depicts a general block diagram of an in-band full-duplex heterodyne transceiver where it can be seen that self-interference cancellation takes place at three stages or levels: at the antenna level, at the analogue level, and at the digital level. At the antenna level, the system can be monostatic where a shared antenna(s) is used to transmit and receive, or it can be bi-static where separate antennas can be used. However, for monostatic systems a duplexing device is required to isolate the transmitted signal from the received signal, such as circulators [4] or hybrid transformers [5]. While, for bistatic systems, the transmit antennas can be placed or fed in a way to create null planes at the positions of the receive antennas which can reduce the coupling between them.

On the other hand, both the analogue and digital cancellation circuitry benefit from the fact that the transmit and receive antennas are co-located on the same board or platform, and therefore, the receiver section has knowledge of the originally transmitted signal and of the characteristics of the
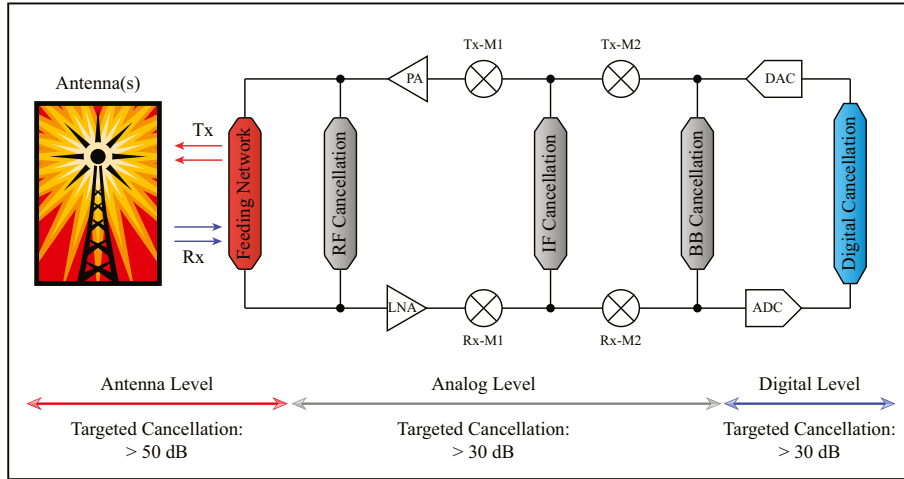
FIGURE 1 General block diagram of an in-band full-duplex transceiver

direct path coupling, which can be predicted and measured. So, a copy of the transmitted signal is taken, and direct path losses and phase changes are applied to it, then it gets subtracted from the received signal [3]. At the analogue level, cancellation can take place at one of three stages: at the RF stage [6] before the amplifiers, then at the intermediate frequency (IF) stage [7], and at the base band (BB) stage [8] before the converters. Note that, it is necessary to suppress the self-interference signals, at the antenna and analogue levels, by at least a certain amount (typically 60 dB [3]) to prevent saturating the analogue-to-digital converter.

The simultaneous transmit-receive property of in-band full-duplex technology can enable the introduction of novel and efficient multiple access techniques [9], physical layer security protocols [10], relaying solutions [11], and can reduce air interface delay [12]. Also, it might benefit radar systems [13], cognitive radios (CR) [14], and multiple-input multiple output (MIMO) arrays [15]. So, considering their appealing advantages, it is highly desirable to implement wideband full-duplex systems for civil, military, and space applications. Available publications on wideband full-duplex systems indicate that achieving 50 dB of self-interference cancellation level over a wide bandwidth is possible at the antenna level [16–18], however, the analogue and digital parts fall far behind with achieving wideband cancellation, mainly, due to circuitry bandwidth limitations and cost. Nevertheless, implementing a wideband full-duplex antenna system remains very attractive as it can be used as a universal transmit-receive system suitable for different standards, frequency bands, or bandwidths, and even for software-defined radios (SDR) or cognitive radios (CR). In light of that, the scope of this work will be mainly focussed on wideband self-interference cancellation techniques at the antenna level.

Several techniques were proposed to attain wideband self-interference cancellation at the antenna level. For monostatic systems, some implementations based on wideband circulators and hybrid transformers can be found in [4, 5], respectively. Nevertheless, the limited isolation of the duplexing

devices limits the maximum achievable level of cancellation. On the other hand, for bistatic systems, the basic technique is to increase the separation between the Tx and Rx antennas [19], however, this results in an increased system size. So, instead, the beams of the antennas can be directed somewhat in different directions to reduce the overlap between them [19], nonetheless, not all applications can tolerate to transmit and receive in different directions. Alternatively, using orthogonal polarisations for the Tx and Rx antennas [20] can increase the level of cancellation, but this requires the Tx antennas of one node to be aligned with the Rx antennas of the other node. Moreover, near-field cancellation [17] showed the capability of achieving a decent level of cancellation with a simple system design and compactness. Also, circularly phased arrays [21–23], can provide a similar performance to near-field cancellation with a quasi-omnidirectional radiation pattern, however, it requires a more complicated feeding network. In addition to all the above, placing high impedance structures between the antennas were considered in [16], which can provide a high level of cancellation, however, the size of such structures can drastically increase the overall size of the system. Finally, based on the above techniques wideband full-duplex arrays were also demonstrated in [24–27]. Note that, one or more techniques can be used in conjunction to achieve the maximum possible level of self-interference cancellation.

In the next section, our system specifications, detailed contributions, and the potential applications of the proposed system will be presented. Then, the whole system with all the individual devices will be presented in Section 3, where its principle of operation will be explained. And in Section 4, the final system assembly, matching, self-interference cancellation, and far-field performance will be demonstrated both in simulations and in measurements. Also, in this section, the new figure of merit will be introduced, and then the section will be closed with a table that compares this work to previous works in the literature, especially in terms of the newly introduced figure of merit.

2 | SCOPE OF WORK

In this work, we aim to design an ultra-wideband in-band full-duplex system with at least 50 dB of self-interference cancellation at the antenna level, that can transmit and receive in the same direction with a fairly high directivity. And as it was evident, from the published works, that bistatic techniques have more wideband potential than monostatic techniques, in particular, near-field cancellation which can satisfy the required specifications if, at the same time, orthogonal polarisations are used for the transmit and receive antennas. And in addition to that, near-field cancellation can generate the most compact full-duplex systems as compared to all other bistatic techniques. However, it requires at least four antennas and two 180° out-of-phase power dividers (or baluns), and it can be sensitive to the baluns' amplitude and phase imbalances, and, also, to the antennas' placement.

Near-field cancellation has been implemented in several previous works, mainly, with planar antennas operating at the low frequency side of the spectrum (below the K-band), and over bandwidths not more than one or two octaves [17, 20, 28–30]. But, in this work, we aim to have a system that can operate up to the Ka-band while covering most of the lower bands (starting from the C-band). To achieve this goal, and to satisfy the previously mentioned specifications, we propose a system that consists of a 4-element Vivaldi array and two microstrip-to-slotline baluns, as depicted in Figure 2. Although the individual devices of the system are planar, yet the system is three-dimensional, which creates some vagueness about the operation of the near-field cancellation technique, taking into consideration that it has only been demonstrated for planar systems. Thus, our work can be considered the first work to implement the near-field cancellation technique over an extremely wide bandwidth with a three-dimensional antenna system, and our contributions can be summarised as follows:

- Achieving 50 dB of self-interference cancellation, at the antenna level, over an extremely wide bandwidth (4–40 GHz).
- Optimising the microstrip-to-slotline transition to operate over the desired bandwidth. The transition will be used to feed the antennas and it constitutes the basic building block of the used baluns.
- Proposing a way to align the antennas using a 3D-printed support.
- Introducing a new figure of merit, the wideband full-duplex systems figure of merit (FoM$_{\text{WFD}}$), to assess the performance of wideband in-band full-duplex systems, and it accounts for the achieved self-interference cancellation level, the gain, the bandwidth, and the size of the system.

The proposed system can be considered for diverse applications where capacity, low latency, and secrecy capabilities, offered by in-band full-duplex, are required. That may concern, for example, in cellular telecommunication systems, backhaul microwave links between the core network and the radio access network, or wireless links between two remote base stations instead of using fibre optic. More broadly, the 'sensing-as-transmitting' property, along with all other characteristics of in-band full-duplex, can be valuable for any wideband multi-standard communication operation especially for cognitive radios which require continuously scanning a wide range of frequencies while transmitting.

3 | SYSTEM DESIGN

3.1 | Principle of operation

The proposed in-band full-duplex system is depicted in Figure 2 where the substrates were omitted for better clarity. The system is composed of four Vivaldi antennas which are placed on the perimeter of a circle of a fixed radius and sequentially rotated by 90° from one another, thus forming two diametrically opposite pairs of antennas, where each pair is orthogonal to the other. One pair is used to transmit, and the other is used to receive. Then each pair of antennas is fed signals of equal amplitudes and 180° out-of-phase by using wideband microstrip-to-slotline baluns. To explain the principle of operation of the proposed system, two approaches are adopted [17]: an inter-port approach that describes the power coupling between the input and output ports of the *Tx* and *Rx* baluns, and a field approach that describes the electric field behaviour in the far-field region.

Inter-Port Approach: in order to develop this approach, we find that it is most suitable to work with power waves [31], where a_n denotes the power wave incident at port n and b_n denotes the power wave reflected from that port, and accordingly, the total powers carried by each wave are equal to $|a_n|^2$ and $|b_n|^2$, respectively. The flow of power waves in the system is depicted in Figure 2b assuming ideal conditions where no mismatch exists between the system components.

Now, the output power (P_o) at the output of the *Rx* balun can be expressed in terms of power waves coming from the receive antennas 1 and 3 as follows:

$$P_o = |b_o|^2 = \left|a_o' + a_o'' e^{j\pi}\right|^2 = \left|b_1 + b_3 e^{j\pi}\right|^2 \qquad (1)$$

Also b_1 and b_3 can be expressed in terms of the power waves incident on the transmit antennas 2 and 4 as follows:
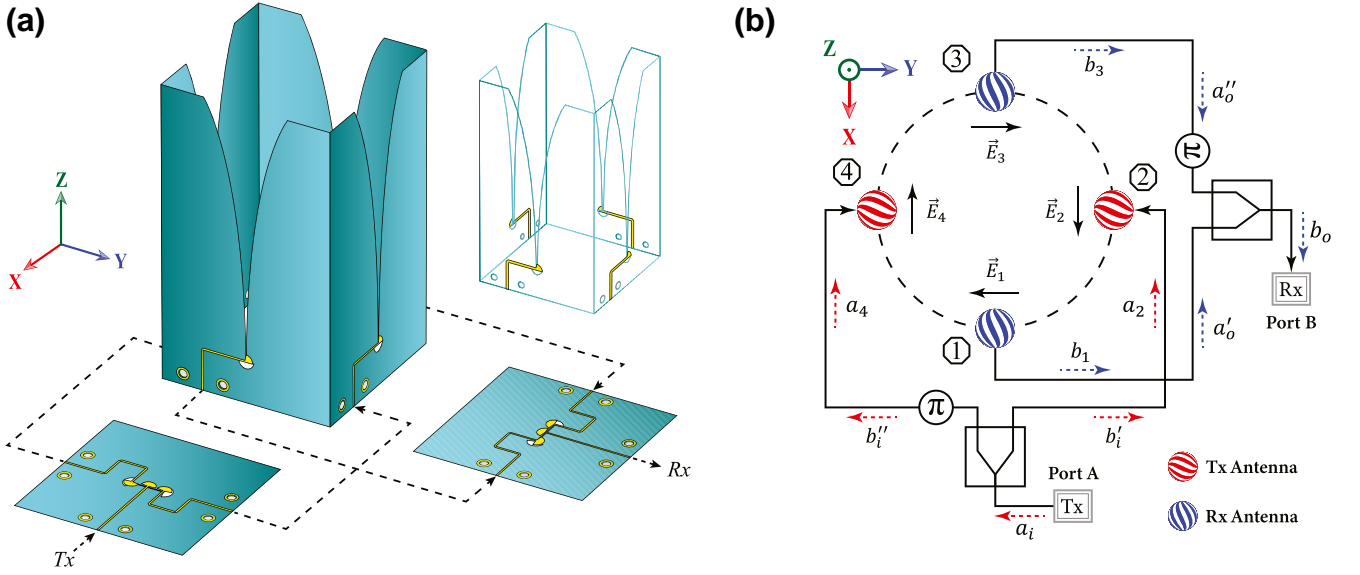
$$b_1 = S_{12}a_2 + S_{14}a_4 \qquad (2)$$

$$b_3 = S_{32}a_2 + S_{34}a_4 \qquad (3)$$

Similarly, a_2 and a_4 can be written in terms of the power wave a_i incident at the input of the *Tx* balun:

$$a_2 = b_i' = \frac{\sqrt{2}}{2}a_i \qquad (4)$$

$$a_4 = b_i'' = \frac{\sqrt{2}}{2}a_i e^{j\pi} \qquad (5)$$

(a)

(b)

FIGURE 2 (a) An illustration of the proposed wideband in-band full-duplex system with 4-element Vivaldi array and two microstrip-to-slotline baluns, and in the background a transparent view of the Vivaldi array showing the position and orientation of the microstrip feed lines. (b) A schematic of the system showing antenna placement and numbering, flow of power waves, and the original electric fields radiated by each single antenna before connecting them to the baluns

By substituting (4) and (5) in (2) and (3) we obtain:

$$b_1 = \frac{\sqrt{2}}{2}S_{12}a_i + \frac{\sqrt{2}}{2}S_{14}a_ie^{j\pi} = \frac{\sqrt{2}}{2}a_i\left(S_{12} + S_{14}e^{j\pi}\right) \quad (6)$$

$$b_3 = \frac{\sqrt{2}}{2}S_{32}a_i + \frac{\sqrt{2}}{2}S_{34}a_ie^{j\pi} = \frac{\sqrt{2}}{2}a_i\left(S_{32} + S_{34}e^{j\pi}\right) \quad (7)$$

Finally, by substituting (6) and (7) in (1) we can obtain the output power (P_o) in terms of the input power (P_i):

$$P_o = \left|\frac{\sqrt{2}}{2}a_i\left(S_{12} + S_{14}e^{j\pi}\right) + \frac{\sqrt{2}}{2}a_i\left(S_{32} + S_{34}e^{j\pi}\right)e^{j\pi}\right|^2$$

$$P_o = \frac{\sqrt{2}}{2}|a_i|^2|S_{12} + S_{14}e^{j\pi} + S_{32}e^{j\pi} + S_{34}e^{j2\pi}|^2$$

$$P_o = \frac{1}{2}P_i|S_{12} - S_{14} - S_{32} + S_{34}|^2 \quad (8)$$

Equation (8) implies that if $S_{12} = S_{14}$ and $S_{32} = S_{34}$, then the power coupled from the input port of the system to the output port will be equal to zero. This means that if the Rx antennas are placed along the perpendicular bisector of the Tx antennas, then infinite isolation is, theoretically, obtained between them. This conclusion holds only if the antennas are placed and aligned precisely and if the balun operates ideally, that is if the two output signals of the balun are of equal amplitudes and 180° out-of-phase. Nonetheless, in practice, there will be slight misplacements of antennas and imbalances in the amplitude and phase of the balun's output signals, thus the isolation between the

input and the output ports of the system is expected to decrease.

Field Approach: Assuming that the antennas are not connected to the baluns, then each individual antenna element radiates a linearly polarised electric field of magnitude E_0 which is oriented in the opposite direction of the microstrip stub orientation, Figure 2b. So, the individual electric fields can be expressed as follows:

$$\vec{E}_1 = E_0e^{j\pi}\vec{y} \quad (9)$$

$$\vec{E}_2 = E_0\vec{x} \quad (10)$$

$$\vec{E}_3 = E_0\vec{y} \quad (11)$$

$$\vec{E}_4 = E_0e^{j\pi}\vec{x} \quad (12)$$

Now, if the baluns are connected to the antennas, then the Tx and Rx electric fields can be described as follows:

$$\vec{E}_{Tx} = \vec{E}_2 + \vec{E}_4e^{j\pi} = 2E_0\vec{x} \quad (13)$$

$$\vec{E}_{Rx} = \vec{E}_1 + \vec{E}_3e^{j\pi} = 2E_0e^{j\pi}\vec{y} = -2E_0\vec{y} \quad (14)$$

Equation (13) implies that the electric fields of the two transmit antennas will combine constructively in the far-field region and Equation (14) implies the same observation for the receive antennas. However, this conclusion only holds if each two opposite antennas are symmetrically rotated with respect to the centre of symmetry of the system, that is, their

feeding microstrip lines are oriented in opposite directions (see the background image in Figure 2a), and if the antennas are fed signals that are 180° out-of-phase. The antenna rotation (or feeding line opposite orientation) condition is especially critical, otherwise, electric fields will combine destructively in the far-field, which creates a far-field null, and thus the system will not be able to transmit or receive in the direction of this null.

Note that if the system is not symmetric, that is, if the number of transmit and receive antennas is not the same or if they are fed differently, differences between the transmit and receive far-field radiation patterns will emerge, thus it is extremely favourable to maintain high symmetry in the system. The antennas can be tangent or normal to the circle or could form any angle with the circle in general and can still achieve the same level of self-interference cancellation, however, this affects the total size of the system and the orientation of the radiation pattern. In addition to that, significant grating lobes can be observed in the far-field radiation pattern if the separation between the opposite antennas is greater than a half-wavelength at a certain frequency.

3.2 | Wideband balun design

The initial design of the wideband balun used here was proposed by Rhode et al. [32] and it consists of three microstrip-to-slotline transitions terminated with radial stubs as in Figure 3. The balun operates as follows: the input power is first injected in the middle microstrip line and is then coupled to the slotline at its centre. After that, in the slotline, the power will be divided equally between the left and right paths, and at the end of each path, the power will be coupled again to the
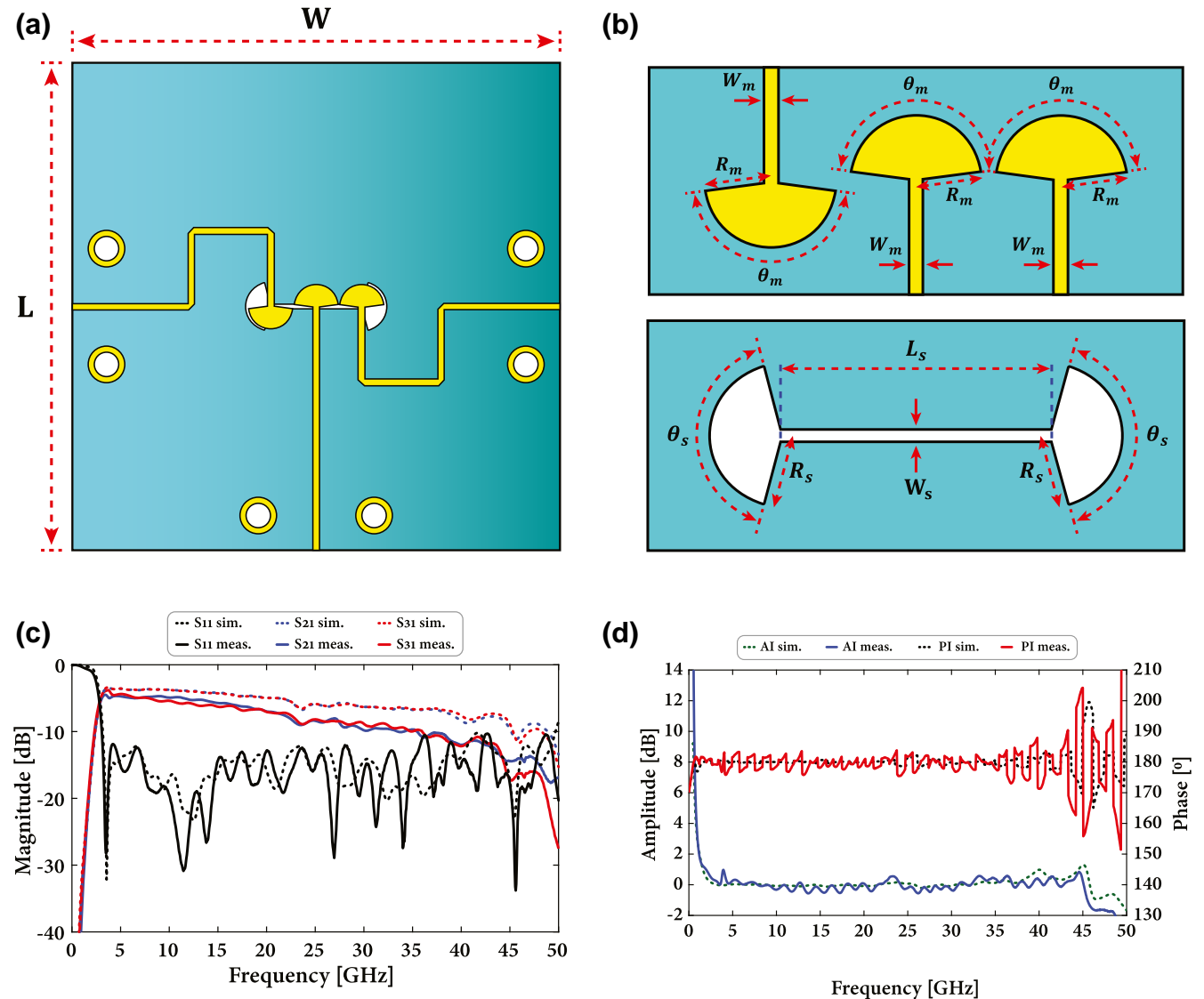
FIGURE 3 (a) Illustrative drawing of the microstrip-to-slotline balun with (b) the parameters of the design. (c) Simulated and measured input matching and insertion losses, and (d) amplitude imbalances (AI) and phase imbalances (PI) between the output ports. {$L = 40$ mm, $W = 40$ mm, $Wm = 0.4$ mm, $R_m = 1.73$ mm, $\theta_m = 165°$, $W_s = 0.1$ mm, $L_s = 8$ mm, $R_s = 1.93$ mm, $\theta_s = 150°$}

corresponding output microstrip line. Since the two output microstrip lines are oriented in opposite directions, the two output signals will be inverted with respect to one another over a wide bandwidth. The used balun was designed and optimised, in CST Microwave Studio, based on the parametric analysis performed by us in [33], after that, two baluns were fabricated on a 203.2 μm thick RO4003C substrate ($\varepsilon_r = 3.55$), and they occupy an area of 40 mm × 40 mm.

The measured S-parameters in Figure 3c show that the balun is matched from 4 to 50 GHz, where a relatively good agreement with simulated results is observed below 30 GHz, while some unexpected jumps in the matching response start to appear beyond 30 GHz. This might probably come from the limitations of the high frequency cables and/or connectors used to conduct the measurements, nevertheless, none of these jumps go higher than −10 dB. Also, the measured insertion loss attains a value of −5 dB at 4 GHz and reaches a value of −11 dB at 40 GHz, however, 3 dB of the insertion loss come from the power division taking place and are not actually lost in the balun. The measured insertion loss drastically increases with frequency as compared to the simulated one, this means that in practice more power is being lost or absorbed by the substrate. This may come from a slight degradation of the substrate characteristics during the fabrication process which led to an increase in the value of its loss tangent (tanδ).

Moreover Figure 3d shows that the amplitude and phase imbalances between the output ports of the balun are less than ±1 dB and ±7° respectively over the 4–40 GHz band, where more fluctuations in the measured results are observed as compared to the simulated results, which might also be attributed to fabrication imperfections. In addition to that, poor levels of matching and isolation between output ports were observed (but not plotted here), which are considered normal as a result of the fact that a 3-port device cannot be lossless, reciprocal, and matched at all ports at the same time. However, simulations proved that low or high levels of isolation between output ports of the balun do not affect the level of self-interference cancellation obtained in the in-band full-duplex system.

3.3 | Wideband Vivaldi antenna design

The Vivaldi antenna, Figure 4, is a uniplanar exponentially tapered slot antenna which is characterised by its wide
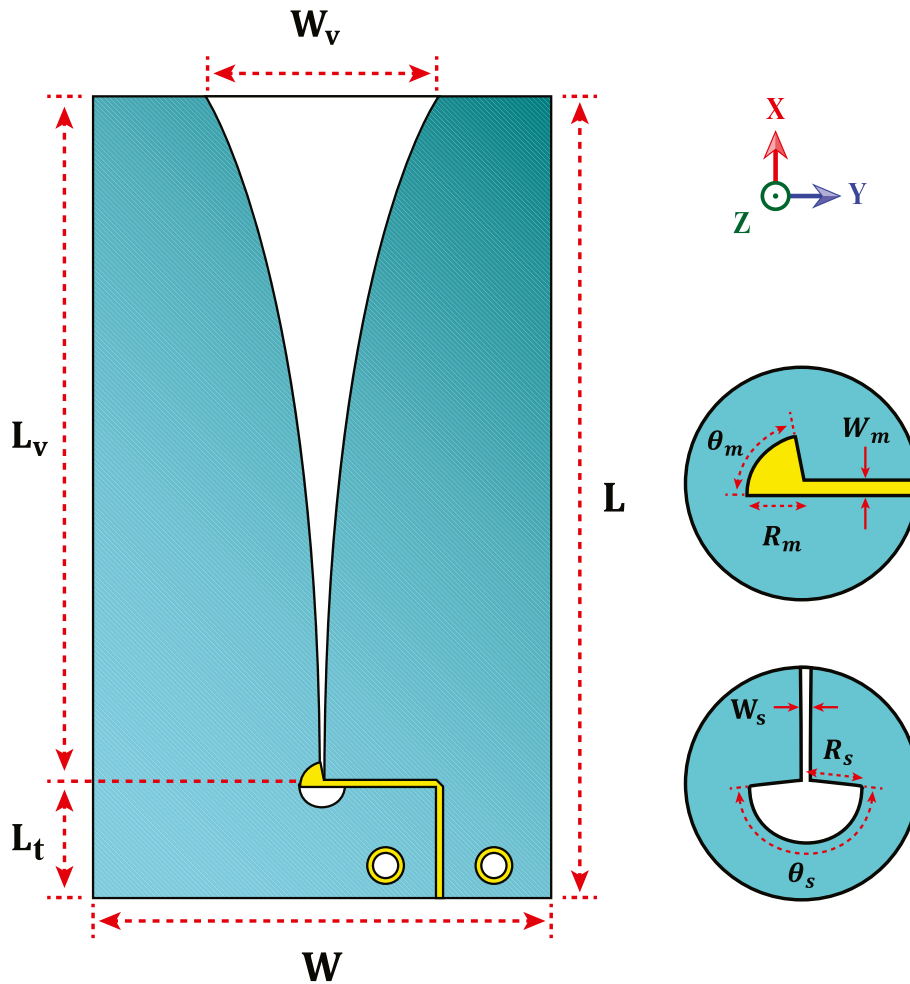
FIGURE 4 Illustrative drawing of the Vivaldi antenna {$L = 70$ mm, $W = 40$ mm, $L_t = 10$ mm, $L_v = 60$ mm, $W_v = 20$ mm, $W_m = 0.4$ mm, $R_m = 1.87$ mm, $\theta_m = 80°$, $W_s = 0.1$ mm, $R_s = 1.85$ mm, $\theta_s = 170°$}

bandwidth, simplicity of its design, its low cost, and its highly directive far-field radiation pattern. The antenna is formed of a microstrip-to-slotline transition acting as a feeding mechanism, and an exponentially tapered slotline acting as a radiating element. The microstrip-to-slotline transition was designed, optimised, and used, previously, in the balun design with a matching bandwidth from below 4 GHz to beyond 40 GHz. So the same transition will be used to feed the Vivaldi antenna, however, note that, a microstrip radial stub with half the size of that used in the balun is adopted here. The size reduction of the microstrip stub reduces the overlap with the slotline stub and, consequently, reduces the power leaked by the transition [33], which means that more power will be fed to the antenna, and this will enhance its efficiency.

On the other hand, the exponential taper can be defined by the following set of equations:

$$y = Ae^{\alpha x} + B \tag{15}$$

$$A = \frac{0.5(W_v - W_s)}{e^{\alpha L} - e^{\alpha L_t}} \tag{16}$$

$$B = \frac{0.5\left(W_s e^{\alpha L} - W_v e^{\alpha L_t}\right)}{e^{\alpha L} - e^{\alpha L_t}} \tag{17}$$

where α is the growth rate of the exponential taper which can be tuned to obtain different antenna characteristics (bandwidth, beamwidth, and gain). In this design, α was set to 0.05 for maximum matching bandwidth. Also, in order for the radiating element to be matched in the same bandwidth as that of the transition, the length of the exponential taper (L_v) was set to approximately one wavelength at 4 GHz, and the aperture width (W_v) was set to approximately a half-wavelength at the central frequency (22 GHz).

The antennas were also fabricated on the same RO4003C substrate ($\varepsilon_r = 3.55$ and $h = 203.2$ μm) where the total size of each antenna element is 70 mm × 40 mm. Figure 5a confirms that the antenna is matched, as expected, from 4 to 47 GHz. And Figure 5b shows that the maximum realised gain of the antenna is better than 5 dBi over the entire matching bandwidth (4–47 GHz) and better than 10 dBi between 7 and 40 GHz in measurements. The Vivaldi gain measurements were performed using three reference antennas to cover the entire matching bandwidth: the first antenna operates in the 2–18 GHz band, the second antenna operates in the 18–33 GHz band, and the third antenna covers the 33–50 GHz band. The three measured gains are depicted in Figure 5b in three different colours: red, blue, and green respectively, while the simulated gain is plotted in black. It is observed that the measured gain is slightly shifted towards the lower frequency side as compared to the simulated gain, which results from fabrication imperfections, however, the shape of the measured curve is highly similar to the simulated curve.
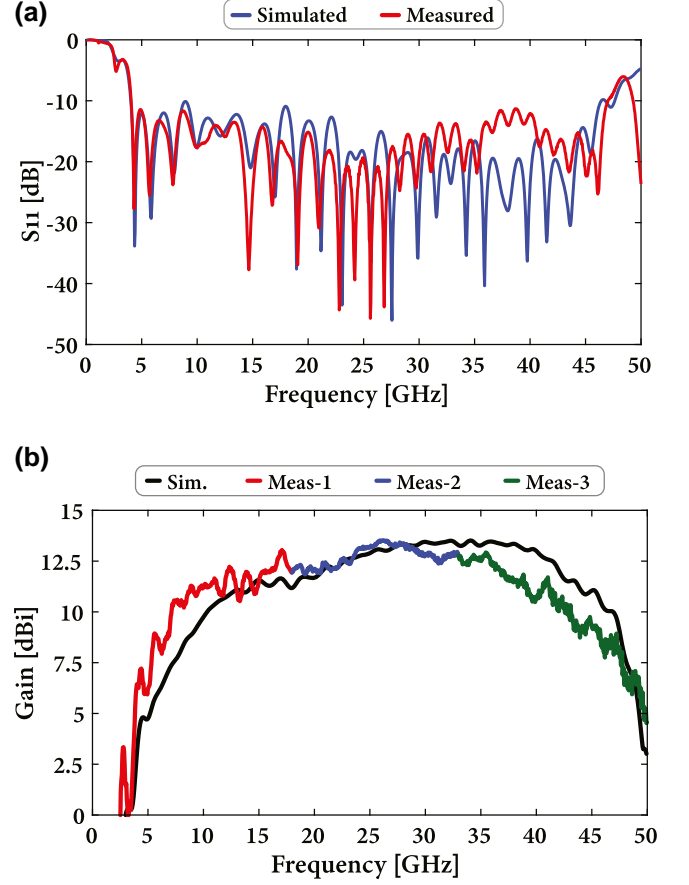

FIGURE 5 Simulated and measured (a) matching and (b) broadside maximum realised gain of the designed Vivaldi antenna

4 | SYSTEM ASSEMBLY AND PERFORMANCE

4.1 | System assembly

To achieve self-interference cancellation and ensure proper system performance, it is of great importance to preserve a high symmetry when assembling the system, that is, the antennas should be placed exactly at the same distance away from the centre of symmetry. While it is easy to place the antennas precisely and symmetrically in a simulation environment, yet, in practice it cannot be guaranteed. Moreover, it was noticed that the fabricated antennas tend to bend naturally due to the low thickness of the used substrate (203.2 μm), which also contributes to the asymmetry of the system. Also, the thickness of the substrate makes it very fragile and prone to fracturing, mainly, due to the tension exerted by the feeding cables and connectors. To resolve those mechanical issues, a 3D-printed support is designed and fabricated to ensure precise antenna placement, to reduce antenna bending and to hold it fully erect, and to absorb mechanical tension from the feeding cables and connectors.

Figure 6b depicts the 3D-printed support which was made of Polyvinyl-Chloride (PVC, $\varepsilon_r \approx 3$), and the different parts of the support were fixed together using PTFE screws ($\varepsilon_r \approx 2.1$). The support is designed such that it only grasps the edges of the antennas and is kept sufficiently below the top of the antenna. This ensures that the support will not affect the antennas' matching or performance. But before installing the antennas inside the 3D-printed support, Southwest 2.92 mm connectors were mounted on all devices, and four Keysight N5448B phase-paired cables (± 5 ps skew) were used to connect the antennas to the baluns. However, note here that the fabricated baluns were modified slightly to have their output ports at the top (as shown in Figure 6a), which makes it easier to connect them directly to the antennas as shown in Figure 6c and 6d. Finally, the measurements were carried out by using Rhode&Schwarz ZVA67 vector network analyser.

4.2 | System performance

The simulated and measured characteristics of the system are depicted in Figure 7. Note that simulations were done taking into account the PTFE screws and the 3D-printed support, which was modelled as a lossless dielectric material having $\varepsilon_r \approx 3$. Also, simulations take into account the extra separation distance between the antennas as per the fabricated design in Figure 6b. Moreover, in simulation, the phase-paired cables were modelled as straight pieces of coaxial lines (25 cm long) formed of aluminium inner and outer conductors and PTFE dielectric stuffing. In addition to that, the 2.92 mm connectors were not considered in simulations. And finally, note that the baluns that were considered in simulations are the simulated microstrip-to-slotline baluns and not some ideal baluns, which means that the signals entering the antennas are not ideal, that is they are not perfectly of equal amplitudes and 180° out-of-phase, but rather they are subject to the phase and amplitude imbalances of the simulated baluns.

4.2.1 | System matching

Figure 7a shows that the assembled in-band full-duplex system has a return loss better than 10 dB over an ultra-wide frequency band (3.5–49.35 GHz). The measured matching seems to be slightly better than the simulated one around some frequencies, and this can be attributed to the higher insertion losses of the fabricated baluns, and also to the power losses resulting from the phase-paired cables and the 2.92 mm connectors. While these losses reflect positively on the system's matching, yet they will reflect negatively on the measured gain of the system, which is depicted in Figure 7c.
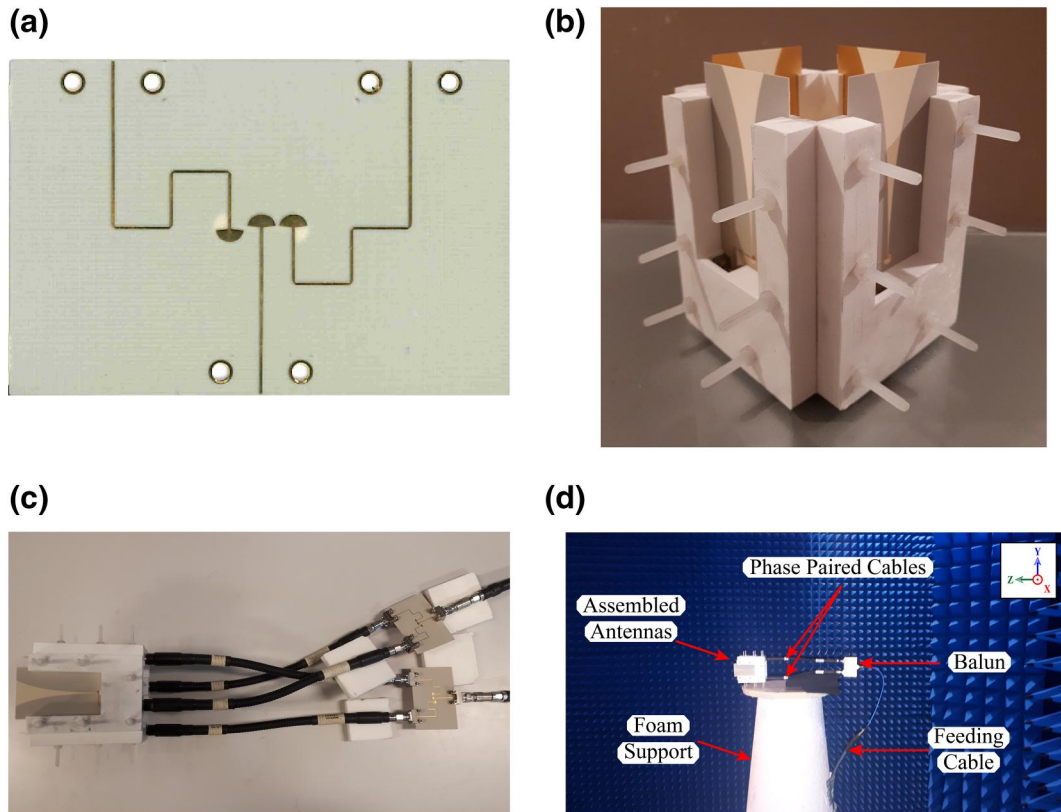
FIGURE 6 Pictures of (a) the fabricated balun, (b) antenna assembly inside the 3D-printed support, (c) whole system assembly and (d) measurements inside the anechoic chamber
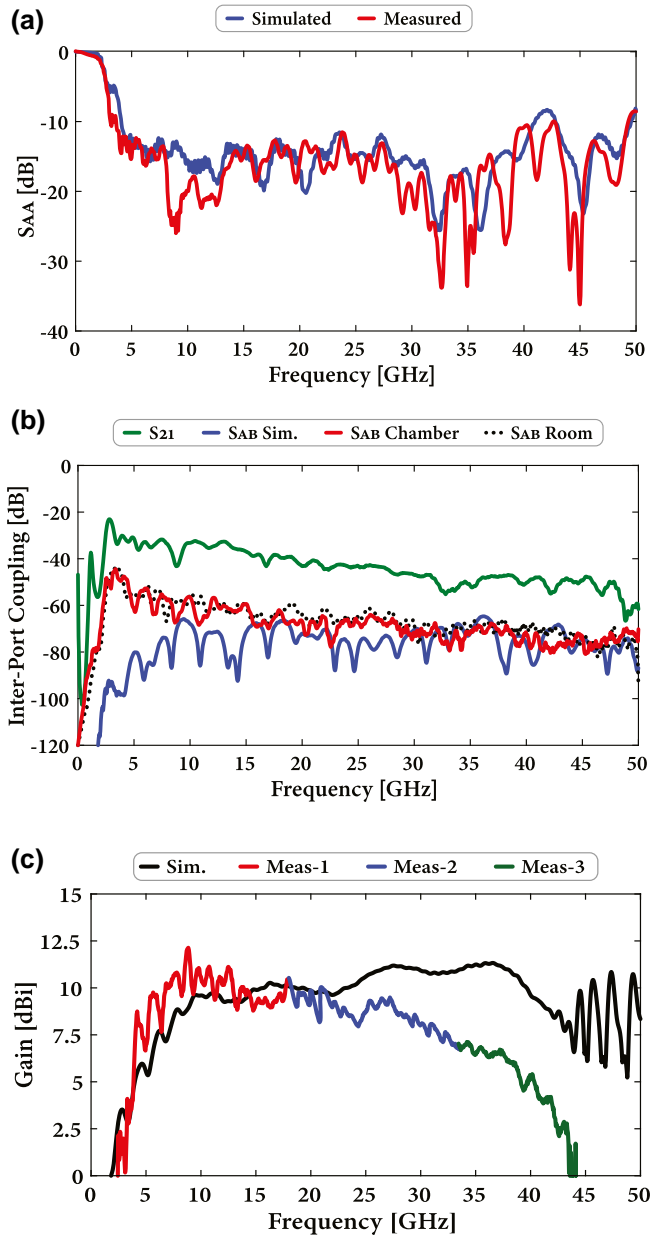
FIGURE 7 The proposed in-band full-duplex system (a) matching, (b) inter-port coupling, and (c) broadside maximum realised gain

4.2.2 | Self-interference cancellation

Figure 7b depicts the inter-port coupling (or the insertion loss) between the different ports of the system. Note that self-interference cancellation is equal to the negative of the inter-port coupling (in dB). In fact, inter-port coupling and self-interference cancellation express similar meanings in opposite senses. Inter-port coupling tells how much of the power incident at the input port is transmitted to the output port, while self-interference cancellation tells by how much the power transmitted to the output port is weaker than the power incident at the input port, or inversely, it tells by how much the power incident at the input port is stronger than the power transmitted to the output port. The different plots in Figure 7b are explained below:

- "S_{21}" is the coupling (or cross-polarisation) between the two orthogonal antennas 1 and 2 in Figure 2b if they are excited individually without a balun. And the aim of this measurement is to see how much cancellation is initially obtained from the fact that the transmit and receive antennas are orthogonally polarised.
- "S_{AB} Sim." is the simulated coupling between the input port of the Tx balun (Port A) and the output port of the Rx balun (Port B).
- "S_{AB} Chamber" is the measured coupling between the input port of the Tx balun (Port A) and the output port of the Rx balun (Port B) inside the anechoic chamber.
- "S_{AB} Room" is the measured coupling between the input port of the Tx balun (Port A) and the output port of the Rx balun (Port B) in a normal room that has no electromagnetic insulation and that contains many objects (chairs, tables, instruments, etc.) which might cause multipath reflections. The purpose of this measurement is to compare its result to the one obtained in the anechoic chamber, and to see if the reflections from the surrounding environment have any effect on the performance of the system.

Now, the measured level of self-interference cancellation for the whole system in the anechoic chamber is about 50 dB at 4 GHz and reaches about 70 dB at 40 GHz, while in simulation it starts with 80 dB at 4 GHz and continues to maintain approximately the same value until it reaches 40 GHz. The lower level of cancellation in measurements was expected as a result of fabrication imperfections, antenna misplacement in the 3D-printed support, and the higher imbalances in the phases and amplitudes of the baluns. Also, if we compare the system cancellation, which was obtained in the anechoic chamber, to the measured cancellation between the two orthogonal antennas 1 and 2, which is 30.5 dB at 4 GHz and 50.5 at 40 GHz, we can notice that the used cancellation technique, with differential feeding, can provide, at least, an extra 20 dB of cancellation, on average, on the top of the cancellation obtained from cross-polarisation. Finally, by comparing the system cancellation in the anechoic chamber to the system cancellation in a normal room, we can notice that the difference between the two is almost negligible. This indicates that the reflections from the surrounding environment are less significant than the residual self-interference, and therefore, have a negligible effect on the cancellation performance of the proposed system.

4.2.3 | Farfield performance

The gain of the system is depicted in Figure 7c where it can be seen that there are some differences between the simulated and measured results. In fact, the simulated gain starts with a value of 4.5 dBi at 4 GHz and then starts to increase with frequency. It reaches a value of 10 dBi around 10 GHz and continues to maintain almost the same value throughout the rest of the bandwidth. Finally, it starts to drop again around 40 GHz. On the other hand, the measured gain starts with a value of 5 dBi

at 4 GHz and then it continues to increase with frequency and reaches its peak value (about 10 dBi) around 10 GHz. From that point, the measured gain starts to drop with frequency until it hits 5 dBi at 40 GHz. The drop in the measured gain can be attributed to the higher insertion losses of the fabricated balun and also to the power losses resulting from the phase-paired cables and the 2.92 mm connectors, which were not considered in simulations. However the measured gain remains higher or equal to 5 dBi in the bandwidth of matching (4–40 GHz), and the average gain in this bandwidth is 7.8 ± 2.6 dBi.

In addition to that, Figure 8a, 8b, 8c and 8d depict some sample radiation pattern plots at 5, 15, 25, and 35 GHz, respectively, where good agreement between simulated and measured results is observed. The radiation pattern plots reveal that a directive main lobe is present in the yz-plane, and that at least two grating lobes are present alongside the main lobe in the xz-plane. And it seems that the number of grating lobes increases as we go higher in frequency. In fact, at least two grating lobes start to appear in the radiation pattern when the separation distance between the two opposite antennas is higher than a half-wavelength at the frequency of measurement, and their number increases when the separation becomes higher than a multiple of half-wavelength. Similar results were observed in other publications on near-field cancellation [17], and in publications on Vivaldi arrays [34]. This phenomenon can be considered as a major drawback of

the system, though it cannot be avoided unless the separation distance between the antennas is reduced. However, for the presented Vivaldi array, this cannot be feasible because the separation distance is conditioned by the width of the single antenna element, which is usually equal or greater than a wavelength at the central frequency. This means, for such wideband system, whatever the antenna width is, there will always be a portion of the bandwidth (the higher frequency range) where the grating lobes are present.

4.3 | Figure of merit

To assess the merits of the proposed system a new figure of merit, wideband full-duplex figure of merit (FoM$_{\text{WFD}}$), is introduced, and it accounts for the achieved self-interference cancellation level, the gain, the bandwidth, and the normalised size of the system. Firstly, both the values of the self-interference cancellation and the gain of the system should be linear and not in dB, however, note that the dB value of the self-interference cancellation should be positive before converting it to a linear scale. Secondly, concerning the size of the system, some systems have a two-dimensional geometry, such as systems fabricated on printed-circuit boards (PCBs) where the thickness of the substrate is almost negligible, while other systems possess a three-dimensional geometry, which is the case for our system, also, some systems have their feeding
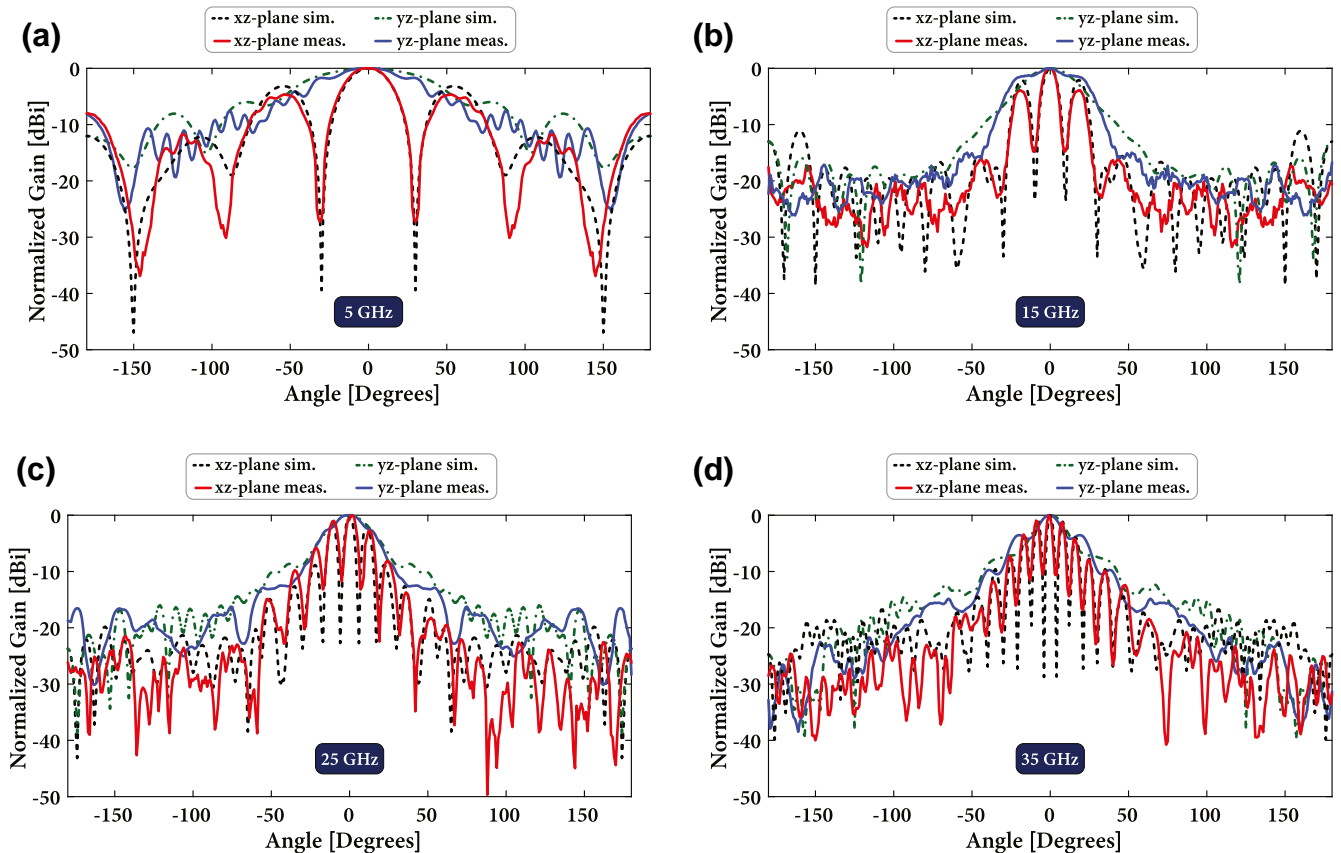

FIGURE 8 Radiation pattern plots at (a) 5 GHz, (b) 15 GHz, (c) 25 GHz, and (d) 35 GHz, respectively

network directly integrated on the same board or platform while other systems have their feeding networks built on separate boards and connected with cables. These differences make it difficult to find a common and fair way to compare sizes of different systems, so here we propose a method which is based on three points: (a) we let the system be inscribed in a sphere of radius R, this radius will be used in the figure of merit to represent the size of the system, (b) if the feeding network is integrated with the antennas on the same board then it will be accounted for in the size calculation, and, otherwise, it will be disregarded, (c) after calculating the radius of the sphere it will be normalised by the wavelength at the centre frequency. Based on all the above, the figure of merit is expressed as follows:

$$\text{FoM}_{\text{WFD}} = \log_{10}\left(\frac{\text{SIC} \times \text{Gain} \times \text{FBW}}{R/\lambda_c}\right) \quad (18)$$

$$\text{FBW} = \frac{f_u - f_l}{f_c} \quad (19)$$

$$R = \frac{1}{2}\sqrt{l^2 + w^2 + h^2} \quad (20)$$

SIC: average self-interference cancellation level.
Gain: average system gain.
FBW: fractional bandwidth.
f_u: upper frequency.
f_l: lower frequency.
f_c: central frequency.
λ_c: wavelength at the central frequency.
R: radius of the sphere circumscribing the full-duplex system.
l: length of the full-duplex system.
w: width of the full-duplex system.
h: height of the full-duplex system.

The proposed figure of merit is an initial attempt to combine different parameters of in-band full-duplex antenna configurations or topologies in an expressive way to evaluate the performances of the proposed systems and compare them to each other. However, depending on the targeted application, it might be modified to incorporate other metrics related to the field of application, such as the type of polarisation, the number of polarisations (singular or dual), number of antennas used, antenna efficiency and level of side lobes, and the performance of the feeding network. Finally, Table 1 compares this work to other in-band full-duplex antenna topologies previously published in the literature, especially in terms of bandwidth, level of self-interference cancellation, system gain and size, and the newly introduced figure of merit where it can be noticed that our proposed system achieves the highest score. Also, up to our knowledge, it works over the widest bandwidth (a decade bandwidth) and reaches the highest upper frequency (40 GHz) which is conditioned by a minimum gain level of 5 dBi, however, otherwise, the highest matching frequency can go up to 49 GHz.

5 | CONCLUSION

In this study, an ultra-wideband full-duplex system consisting of four Vivaldi antennas and two microstrip-to-slotline baluns is presented. The prototype was built on RO4003C substrate ($\varepsilon_r = 3.55$, $\tan\delta = 0.0027$, $h = 203.2$ μm). The proposed system can achieve 50 dB of self-interference cancellation at the antenna level and a gain better than 5 dBi over the 4–40 GHz frequency range with a highly directive radiation pattern, which proves that in-band full-duplex can be extended to ultra-wideband operation. The proposed system is a general-purpose tool that can be used in various applications especially those that require high data-rate links, or reconfigurability over a wide bandwidth. The performance of the proposed system can be further enhanced by considering the following perspectives:

- Due to the relatively high loss tangent of the used substrate and due to fabrication imperfections, the fabricated baluns suffer from high insertion losses, especially at high frequencies, which decreases the total gain of the system. To resolve these issues the baluns and antennas can be designed and fabricated on a different substrate with lower tangent loss, RT/Duroid 5880 ($\varepsilon_r = 2.2$, $\tan\delta = 0.0009$) for example. Our primary simulations confirm that the current matching bandwidth (4–40 GHz) can still be maintained using the latter substrate with a thickness of 0.254 mm.
- Also, integrating the baluns and antennas on the same board is currently under consideration, which allows us to get rid of the phase-paired cables and the 2.92 mm connectors, and that reduces the losses in the system.

TABLE 1 A table comparing several wideband antenna systems for in-band full-duplex applications

Reference	Frequency range (GHz)	FBW	SIC (dB)	Gain (dBi)	l × w × h (cm × cm × cm)	R (cm)	FoM$_{\text{WFD}}$
[4][a]	4–8	0.67	45	25	40 × 40 × 25.3	30.984	4.531
[22][a]	0.5–2	1.2	45	5	20 × 20 × 12.5	15.462	4.77
[23][a]	0.8–1.7	0.72	40	4	60 × 60 × 30	45	3.784
[16][a]	6–19	1.04	60	12	38 × 13 × 19	22.215	4.651
This work	4–40	1.64	64	7.8	8 × 8 × 9.4	7.55	5.072

[a]Some parameters' values were extracted from figures or graphs.

- Moreover, the low substrate thickness is necessary for the wideband performance of the fabricated devices, however, this comes at the expense of the fragility of these devices. To encounter this problem, we designed a 3D-printed support to hold the antennas and absorb any external mechanical tensions. However, as an alternative solution, one can increase the thickness of the substrate while sacrificing a portion of the obtained bandwidth.

- In addition to the above, other than in-band full-duplex applications, the whole system can be used as one dual-polarised antenna array, and the way it is implemented, and fed can greatly enhance the level of cross-polarisation over a very wide bandwidth.

- Finally, the whole system can be used to generate circularly polarised waves by modifying the feeding network. The circular polarisation can be obtained by feeding the four antennas signals having equal amplitudes and having phases of 0°, 90°, 180°, and 270°, consecutively.

ACKNOWLEDGEMENTS

CONFLICT OF INTEREST

The authors declare that there is no conflict of interest.

PERMISSION TO REPRODUCE MATERIALS FROM OTHER SOURCES

None.

DATA AVAILABILITY STATEMENT

The data that support the findings of this study are available from the corresponding author upon reasonable request.

ORCID

Hadi Hijazi https://orcid.org/0000-0001-7337-452X

REFERENCES

1. IT Union: IMT traffic estimates for the years 2020 to 2030. Report ITU (2015)
2. Sabharwal, A., et al.: In-band full-duplex wireless: challenges and opportunities. IEEE J. Sel. Area Commun. 32(9), 1637–1652 (2014)
3. Bharadia, D., McMilin, E., Katti, S.: Full duplex radios. In: Proceedings of the ACM SIGCOMM 2013 Conference on SIGCOMM, pp. 375–386 (2013)
4. Prasannakumar, P.V., Elmansouri, M.A., Filipovic, D.S.: Broadband monostatic simultaneous transmit and receive reflector antenna system. In: 2017 IEEE International Symposium on Antennas and Propagation and USNC/URSI National Radio Science Meeting, pp. 553–554. IEEE (2017)
5. Etellisi, E.A., Elmansouri, M.A., Filipovic, D.S.: Wideband monostatic co- polarized co-channel simultaneous transmit and receive broadside circular array antenna. IEEE Trans. Antenn. Propag. 67(2), 843–852 (2018)
6. Venkatakrishnan, S.B., Alwan, E.A., Volakis, J.L.: Wideband RF self-interference cancellation circuit for phased array simultaneous transmit and receive systems. IEEE Access. 6, 3425–3432 (2018)
7. Van den Broek, D.J., Klumperink, E.A., Nauta, B.: An in-band full-duplex radio receiver with a passive vector modulator downmixer for self-interference cancellation. IEEE J. Solid. State Circ. 50(12), 3003–3014 (2015)
8. Liu, Y., et al.: Digitally assisted analog interference cancellation for in-band full-duplex radios. IEEE Commun. Lett. 21(5), 1079–1082 (2017)
9. Amin, M., Hossain, M., Atiquzzaman, M.: In-band full duplex wireless LANs: medium access control protocols, design issues and their challenges. J. Inf. 11(4), 216 (2020)
10. Van Nguyen, B., Jung, H., Kim, K.: Physical layer security schemes for full- duplex cooperative systems: state of the art and beyond. IEEE Commun. Mag. 56(11), 131–137 (2018)
11. Liu, G., et al.: In-band full-duplex relaying: a survey, research issues and challenges. Commun. Surv. Tutorials, IEEE. 17(2), 500–524 (2015)
12. Debaillie, B., et al.: In-band full-duplex transceiver technology for 5G mobile networks. In: ESSCIRC Conference 2015-41st European Solid-State Circuits Conference (ESSCIRC), pp. 84–87. IEEE (2015)
13. Stove, A.G.: Linear FMCW radar techniques. IEE Proceedings F (Radar and Signal Processing), vol. 139, pp. 343–350. IET (1992)
14. Darabkh, K.A., et al.: A–Z overview of the in-band full-duplex cognitive radio networks. Comput. Commun. 145, 66–95 (2019)
15. Du, X., et al.: MIMO broadcast channel with continuous feedback using full-duplex radios. In: 2014 48th Asilomar Conference on Signals, Systems and Computers, pp. 1701–1705. IEEE (2014)
16. Prasannakumar, P.V., Elmansouri, M.A., Filipovic, D.S.: Wideband decoupling techniques for dual-polarized Bi-static simultaneous transmit and receive antenna subsystem. IEEE Trans. Antenn. Propag. 65(10), 4991–5001 (2017)
17. Wu, J., Li, M., Behdad, N.: A wideband, unidirectional circularly polarized antenna for full-duplex applications. IEEE Trans. Antenn. Propag. 66(3), 1559–1563 (2018)
18. Prasannakumar, P.V., et al.: Wideband quasi-monostatic simultaneous transmit and receive reflector antenna. IEEE Trans. Antenn. Propag. 68(4), 2630–2637 (2019)
19. Everett, E., Sahai, A., Sabharwal, A.: Passive self-interference suppression for full-duplex infrastructure nodes. IEEE Trans. Wireless Commun. 13(2), 680–694 (2014)
20. Ha, J., et al.: Monostatic Co- polarized full-duplex antenna with left-or right-hand circular polarization. IEEE Trans. Antenn. Propag. 65(10), 5103–5111 (2017)
21. Moulder, W.F., Perry, B.T., Herd, J.S.: Wideband Antenna array for simultaneous transmit and receive (STAR) applications. In: 2014 IEEE Antennas and Propagation Society International Symposium (APSURSI), pp. 243–244. IEEE (2014)
22. Lian, R., et al.: A high-isolation, ultra-wideband simultaneous transmit and receive antenna with monopole-like radiation characteristics. IEEE Trans. Antenn. Propag. 66(2), 1002–1007 (2017)
23. Etellisi, E.A., Elmansouri, M.A., Filipovic, D.: Broadband full-duplex monostatic circular-antenna arrays: circular arrays reaching simultaneous transmit and receive operation. IEEE Antenn. Propag. Mag. 60(5), 62–77 (2018)
24. Alwan, E.A., Hovsepian, A., Volakis, J.L.: Ultra-wideband dual polarization arrays with collocated elements for high isolation simultaneous transmit and receive systems. In: 2016 IEEE International Symposium on Phased Array Systems and Technology (PAST), pp. 1–3. IEEE (2016)
25. Hovsepian, A., Alwan, E.A., Volakis, J.L.: Wideband scanning array of spiral antennas for simultaneous transmit and receive (STAR). In: 2017 IEEE International Symposium on Antennas and Propagation and USNC/URSI National Radio Science Meeting, pp. 487–488. IEEE (2017)
26. Zhong, J., Alwan, E.A., Volakis, J.L.: Ultra-wideband dual-linear polarized phased array with 60° scanning for simultaneous transmit and receive systems. In: 2017 International Workshop on Antenna Technology: Small Antennas, Innovative Structures, and Applications (iWAT), pp. 140–141. IEEE (2017)

27. Elmansouri, M.A., Kee, A.J., Filipovic, D.S.: Wideband antenna array for simultaneous transmit and receive (STAR) applications. IEEE Antenn. Wireless Propag. Lett. 16, 1277–1280 (2016)

28. Etellisi, E.A., Elmansouri, M.A., Filipovic, D.S.: Wideband monostatic simultaneous transmit and receive (STAR) antenna. IEEE Trans. Antenn. Propag. 64(1), 6–15 (2015)

29. Etellisi, E.A., Elmansouri, M.A., Filipovic, D.S.: Wideband monostatic spiral array for full-duplex applications. In: 2017 IEEE International Symposium on Antennas and Propagation and USNC/URSI National Radio Science Meeting, pp. 1101–1102. IEEE (2017)

30. Filipovic, D.S., Elmansouri, M., Etellisi, E.A.: On wideband simultaneous transmit and receive (STAR) with a single aperture. In: 2016 IEEE International Symposium on Antennas and Propagation (APSURSI), pp. 1075–1076. IEEE (2016)

31. Kurokawa, K.: Power waves and the scattering matrix. IEEE Trans. Microw. Theor. Tech. 13(2), 194–202 (1965)

32. Rohde, U., et al.: Ultra wide band balun/180° power divider using microstrip-slotline-microstrip transition. In: 2015 IEEE MTT-S International Microwave and RF Conference (IMaRC), pp. 400–404. IEEE (2015)

33. Hijazi, H., et al.: 4-40 GHz in-phase/180° out-of-phase power dividers with enhanced isolation. In: 14th European Conference on Antennas and Propagation–EuCAP 2020, pp. 1–4 (2020)

34. Chan, K.K.M., Tan, A.E.C., Rambabu, K.: Decade bandwidth circularly polarized antenna array. IEEE Trans. Antenn. Propag. 61(11), 5435–5443 (2013)